Nonlinear dynamic analysis of gear systems based on refined dynamic model

Jiahui Yu, Huiyuan Wang*, Dongdong Ren, Jiaxu Yuan and Tongyu Wang
School of Mechatronics Engineering, North University of China, Taiyuan 030051, China
*Email: wanghuiyuan@nuc.edu.cn

ABSTRACT

In order to accurately predict the vibration characteristics of gears, a refined dynamic model for gears is proposed in this study. A novel bearing collision model is established, incorporating nonlinear oil film forces to better simulate bearing collisions during transmission. Additionally, a new gear fractal tooth clearance model is established based on fractal theory and combined with tooth surface roughness. The gear dynamic model is solved using a closed-loop algorithm by combining viscous damping factor and time-varying pressure angle. The responses of different models are compared by the bifurcation diagram, phase portraits, and Poincaré mapping. The result shows that the proposed new bearing model accurately describes bearing collision phenomena compared to traditional bearing models. As the restitution coefficient increases, the system response gradually transitions from periodic to chaotic motion. The stability of the system response decreases with the increase of tooth surface roughness and fractal dimension. Compared with fractal dimension, tooth surface roughness has a more obvious effect on the dynamic response of the system.

Keywords: Bearing collision; dynamic backlash; surface topography; fractal dimension.

1. INTRODUCTION

Gear transmissions are widely utilized in important fields such as aerospace, reducers, and machine tools due to their high efficiency and reliability [1-3]. Gears demonstrate strong dynamic nonlinear characteristics during the meshing process, primarily driven by internal nonlinear dynamic excitations such as time-varying stiffness, meshing damping, and friction. In addition to these direct system parameters, tooth surface topography and bearing collisions have a significant impact on gear transmission characteristics. Therefore, establishing a more refined gear dynamic model is crucial for accurately predicting vibration characteristics during the transmission process.

Due to the unavoidable manufacturing errors, gear meshing surfaces exhibit complex surface topography, which can affect the contact characteristics and ultimately influence the dynamic behavior of the system [4]. In recent years, fractal theory has been extensively utilized as an effective approach to simulate surface morphology in gear dynamics research, especially in investigating the vibration characteristics of gear systems [5] and analyzing multiscale friction behavior [6]. Chen et al. [7] compared the fractal tooth gap model with a gap simulated based on a normal distribution using a pure torque model for gear systems, demonstrating the superior ability of fractal theory to describe variations in tooth clearance. However, such simulation methods have certain limitations, as the average amplitude of the simulated tooth surfaces may vary with the fractal dimension. Thus, they corrected the tooth gap model using surface roughness parameters [8]. Xiang et al. [9] further incorporated fractal tooth surfaces into the nonlinear torsional model of planetary gear transmission systems, discussing the influence of roughness on system response. Yu et al. [10] proposed dynamic fractal contact as an internal excitation and introduced a corresponding closed-loop algorithm to address dynamic challenges in the system. Pan et al. [11] established a fractal wear model for tooth surfaces and compared the vibration responses of systems with dynamic fractal gaps and fixed gaps.

Meanwhile, when considering bearing collisions, it is common in many studies to assume the pressure angle and backlash of gears as constant values [12, 13]. Additionally, the presence of bearing clearances and collisions between bearings and the outer race can lead to variations in the gear center position, thereby affecting parameters such as backlash and meshing pressure angle during the transmission process [14]. Huang et al. [15] presented a gear model to analyze the influence of gear center motion on the system response while assuming a constant pressure angle. Liu et al. [16] conducted a primary investigation on the interaction between bearing clearance and backlash, with the aim of analyzing the specific impact of bearing clearance on dynamic transmission errors. Zhang et al. [17] proposed a gear model to study the effects of bearing clearances on dynamic meshing forces and system vibrations. Kim et al. [18] primarily focused on variations in the

International Conference on Automation and Intelligent Technology (ICAIT 2024), edited by R. Usubamatov, S. Feng, X. Mei,
Proc. of SPIE Vol. 13401, 134010Q · © The Authors. Published under a Creative Commons Attribution CC-BY 3.0 License
doi: 10.1117/12.3051577

system's dynamic response caused by gear translation resulting from bearing collisions. Guo et al. [19] developed a comprehensive dynamic model that considers bearing collisions and analyzed the influence of system parameters on the occurrence of gear pair rattle phenomenon.

In previous studies, the influence of nonlinear bearing collision forces, oil film forces, and dynamic working pressure angles has often been simplified in many gear models. These simplifications have led to the inadequate characterization of the coupled characteristics between backlash, bearing clearances, and gear surface topography. Furthermore, when considering bearings, the Kelvin model fails to accurately describe the bearing forces and energy dissipation during bearing collisions. These factors severely limit the accuracy of nonlinear responses obtained from the models. In this study, we propose a new bearing collision model based on Hertz contact theory and introduce a novel modification form of the Weierstrass-Mandelbrot equation to better describe the surface morphology of gears. The relationship between dynamic pressure angle, surface topography, and bearing clearance was geometrically derived. To address the characteristics of dynamic fractal backlash and nonlinear collisions at bearing locations, a closed-loop algorithm is developed to solve the improved nonlinear dynamic model of the gear system. The effects of various parameters on system response are investigated through the analysis of dynamic transmission errors, hysteresis curves of bearing forces, and maximum gear meshing forces.

2. NONLINEAR GEAR-BEARING COLLISION MODEL

2.1. The centralized mass model

A concentrated mass model of a pair of parallel-axis involute spur gears with tooth and bearing clearances was established, as shown in Figure 1.

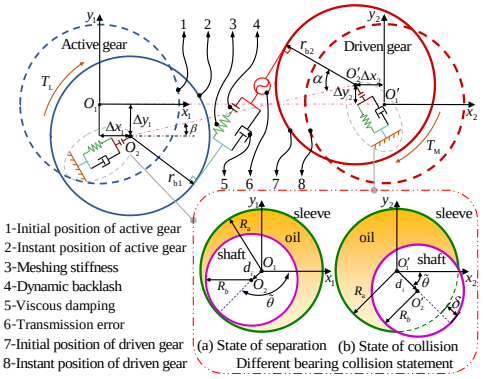

Figure 1. Concentrated mass model of the gear-bearing system.

The gear pair is supported by two sliding bearings. The tooth mesh stiffness k_1 and bearing collision stiffness k_h are indicated by the green springs, and tooth mesh damping c_1 and bearing collision damping c_h are indicated by the pink dampers. The tooth side clearance b_1 and bearing clearance $\xi_i (i=1,2)$ are indicated by the two yellow short lines, while the static transmission error e_1 is indicated by the red marker. $r_{bi} (i=1,2)$ is the radius of the gear base circle, $\Delta x_i (i=1,2)$ and $\Delta y_i (i=1,2)$ are the offset of the gear in the x and y directions, respectively. β is the position angle of a single stage gear. α is the dynamic pressure angle. T_M is the driving torque of the driving gear. T_L is resisting moment.

2.2. Bearing collision model

In the gear model, the bearing collision model is an important component and is usually modeled based on the Kelvin model. However, the Kelvin model has limitations, namely, that the viscous damping coefficient for each collision is set to a constant value throughout the entire collision process. This constant damping coefficient leads to linear and uniform energy dissipation during the penetration and recovery processes in the collision process, which differs from the actual situation [20]. Given the limitations of the Kelvin model, this paper proposes a new nonlinear bearing viscoelastic contact model based on Hertz contact theory to more accurately describe the bearing collision process in the gear model. The simplified bearing contact collision model shows different contact states as shown in figure 1(a) and (b). $O_i (i=1,2)$ and

$O_i'(i=1,2)$ are the center of the bearing outer ring and shaft, respectively. $d_i(i=1,2)$ is the eccentricity vector of the outer ring and shaft of the bearing, R_a and R_b are the radius of the bearing outer ring and shaft respectively.

Due to the existence of bearing clearance, contact and separation occur between the shaft and the outer ring of the bearing, and the magnitude of the impact force can be expressed as:

$$F(t) = k_h \delta^n + \chi \delta^n \dot{\delta} \tag{1}$$

where power exponent $n = 3/2$, k_h represents the contact stiffness of the bearing, which is derived from the Hertz contact theory, while χ represents the viscous damping factor. The contact stiffness of the bearing can be expressed as:

$$k_h = \frac{\pi L_i}{2((1-v_1^2)/E_1 + (1-v_2^2)/E_2)} \sqrt{\frac{1}{2(b_{bi}+\delta_i)}} \tag{2}$$

where $E_i(i=1,2)$ is elastic modulus, $v_i(i=1,2)$ is poisson's ratio.

Lankarani [21] calculated the hysteresis damping factor based on the conservation of momentum and energy. This contact force model is satisfactory in describing energy dissipation during the contact process [22]. The viscous damping factor can be expressed as:

$$\chi = \frac{3(1-\eta^2)}{4} \frac{k_h}{\dot{\delta}^{(-)}} \tag{3}$$

where η is restitution coefficient, b_{bi} is bearing clearance, $\delta_i(i=1,2)$ is penetration depth, $\dot{\delta}_i$ is contact velocity, $\dot{\delta}_i^{(-)}$ is initial impact velocity, $L_i(i=1,2)$ is bearing length.

The embedding depth δ_i and embedding velocity $\dot{\delta}_i$ are expressed by the following functions:

$$\delta_i = \begin{cases} d_i - b_{bi}, & d_i > b_{bi} \\ 0 \quad , & -b_{bi} < d < b_{bi} \\ d_i + b_{bi}, & d_i < -b_{bi} \end{cases} \tag{4}$$

$$\dot{\delta}_i = \begin{cases} \dot{\delta}_i & |\delta_i| > \xi_i \\ 0 & |\delta_i| \le \xi_i \end{cases} \tag{5}$$

In the collision process, the angle $\tilde{\theta}_i$ between the eccentricity vector d_i and the x-axis is constantly changing. The *x* and *y* components of the bearing force on a single gear *i* can be expressed as:

$$\begin{bmatrix} \bar{F}_{xi} \\ \bar{F}_{yi} \end{bmatrix} = \left[\left(\frac{\pi L}{2((1-v_1^2)/E_1 + (1-v_2^2)/E_2)} \sqrt{\frac{1}{2(b_{bi}+\delta_i)}} \right) \left(1 + \frac{3(1-\eta^2)}{4} \frac{k_h \dot{\delta}_i}{\dot{\delta}_i^{(-)}} \right) \delta_i^{\frac{3}{2}} \right] \begin{bmatrix} \cos\tilde{\theta}_i \\ \sin\tilde{\theta}_i \end{bmatrix} \tag{6}$$

2.3. Nonlinear oil film force

In the gear system studied in this paper, sliding bearings are used as the type of bearings. Due to the strong nonlinearity of the non-linear oil film force of sliding bearings, the influence of this factor on the dynamic stability of the system is fully considered in the modeling process of this paper. The classical Capone model [23] is used to describe the non-linear oil film force in this gear system. The oil film force distribution of the sliding bearing is described by the Reynolds equation, and its dimensionless form is expressed as follows:

$$K_i^2 \frac{\partial}{\partial z_i} \left(h^3 \frac{\partial p}{\partial z_i} \right) = \Delta x_i \sin\vartheta - \Delta y_i \cos\vartheta - 2(\Delta \dot{x}_i \cos\vartheta + \Delta \dot{y}_i \sin\vartheta) \tag{7}$$

where $K_i = \tilde{D}_i / L_i$, $\tilde{D}_i (i = 1,2)$ is bearing diameter, L_i represents the length of the bearing, $z_i = \overline{z}_i / L_i$, $\overline{z}_i$ is the axial position coordinate, ϑ is the rotational angle starting from the x-direction of the bearing center, $h_i = \tilde{c}_i / C_i$, $\tilde{c}_i$ is the thickness of the oil film, C_i is radial clearance. p is the dimensionless oil film pressure, p can be expressed by:

$$p = \frac{1}{2}\left[\frac{L_i}{\tilde{D}_i}\right]^2 \frac{(\Delta x_i - 2\Delta\dot{y}_i)\sin\vartheta - (\Delta y_i + 2\Delta\dot{x}_i)\cos\vartheta}{(1 - \Delta x_i \cos\vartheta - \Delta y_i \sin\vartheta)^3}(4z_i^2 - 1) \tag{8}$$

The hydrodynamic dimensionless thrust f_{xi} and f_{yi} of the gear can be expressed as follows:

$$\begin{bmatrix} f_{xi} \\ f_{yi} \end{bmatrix} = \frac{\left[(\Delta x_i - 2\Delta\dot{y}_i)^2 + (\Delta y_i - 2\Delta\dot{x}_i)^2\right]}{1 - \Delta x_i^2 - \Delta y_i^2} \begin{bmatrix} 3\Delta x_i V(\Delta x_i, \Delta y_i, \tilde{\alpha}) - \sin\tilde{\alpha} G(\Delta x_i, \Delta y_i, \tilde{\alpha}) - 2\cos\tilde{\alpha} S(\Delta x_i, \Delta y_i, \tilde{\alpha}) \\ 3\Delta y_i V(\Delta x_i, \Delta y_i, \tilde{\alpha}) + \cos\tilde{\alpha} G(\Delta x_i, \Delta y_i, \tilde{\alpha}) - 2\sin\tilde{\alpha} S(\Delta x_i, \Delta y_i, \tilde{\alpha}) \end{bmatrix} \tag{9}$$

where

$$V(\Delta x_i, \Delta y_i, \tilde{\alpha}) = \frac{2 + (\Delta y_i \cos\tilde{\alpha} - \Delta x_i \sin\tilde{\alpha}) G(\Delta x_i, \Delta y_i, \tilde{\alpha})}{1 - \Delta x_i^{\,2} - \Delta y_i^{\,2}} \tag{10}$$

$$S(\Delta x_i, \Delta y_i, \tilde{\alpha}) = \frac{\Delta x_i \cos\tilde{\alpha} + \Delta y_i \sin\tilde{\alpha}}{1 - (\Delta x_i \cos\tilde{\alpha} + \Delta y_i \sin\tilde{\alpha})^2} \tag{11}$$

$$G(\Delta x_i, \Delta y_i, \tilde{\alpha}) = \frac{2}{\left(1 - \Delta x_i^{\,2} - \Delta y_i^{\,2}\right)^{1/2}} \left[\frac{\pi}{2} + \arctan\frac{\Delta y_i \cos\tilde{\alpha} - \Delta x_i \sin\tilde{\alpha}}{\left(1 - \Delta x_i^{\,2} - \Delta y_i^{\,2}\right)^{1/2}}\right] \tag{12}$$

$$\tilde{\alpha} = \arctan\left(\frac{\Delta y_i + 2\Delta\dot{x}_i}{\Delta x_i - 2\Delta\dot{y}_i}\right) - \frac{\pi}{2}\operatorname{sign}\left(\frac{\Delta y_i + 2\Delta\dot{x}_i}{\Delta x_i - 2\Delta\dot{y}_i}\right) - \frac{\pi}{2}\operatorname{sign}(\Delta y_i + 2\Delta\dot{x}_i) \tag{13}$$

Therefore, the actual force components $\tilde{F}_{xi}$ and $\tilde{F}_{yi}$ in the *x* and *y* directions of the nonlinear oil film force on a single gear *i* can be obtained, which can be respectively represented as:

$$\begin{bmatrix} \tilde{F}_{xi} \\ \tilde{F}_{yi} \end{bmatrix} = \sigma_i \begin{bmatrix} f_{xi} \\ f_{yi} \end{bmatrix} \tag{14}$$

$$\sigma_i = \mu\omega \frac{\tilde{D}_i}{2} L_i \left(\frac{\tilde{D}_i}{2\tilde{c}_i}\right)^2 \left(\frac{L_i}{\tilde{D}_i}\right)^2 \tag{15}$$

where σ_i is the correction factor, μ is the dynamic viscosity of the oil film.

2.4. Dynamic backlash and bearing clearance coupling for fractal characteristics

2.4.1 Dynamic backlash with fractal characteristics

There are objective randomness, multi-scale and self-affinity in the machining process of various types of gear surfaces with different precisions, so that they have certain fractal characteristics. It is verified that the fractal theory is effective to describe the machined surface profile [7], so the Weierstrass-Mandelbrot function can be used to simulate the trend of the concave and convex height of the gear surface morphology. The height of surface asperities is as follows:

$$z_1(t) = \sum_{i=0}^{\infty} \lambda^{(D-2)i} \sin(\lambda^i t) \tag{16}$$

where λ is the characteristic scale coefficient, *D* is the fractal dimension, and the value of *D* is between 1.1 and 1.9.

Clearly, although the value of the backlash is influenced by the surface topography simulated by equation (16), the aforementioned fractal backlash model exhibits changes in the overall amplitude of the micro protrusions on the gear surface when varying the fractal dimension. Consequently, it fails to accurately describe the overall morphology changes in the contact area under the same roughness conditions. To address this issue, we introduce a correction coefficient obtained by considering the absolute values of all micro protrusion heights within the calculation interval and the gear surface roughness, which is then incorporated into the new modified fractal gap model. The correction coefficient of the model can be expressed as：

$$\varphi = \frac{nTRa}{\int_0^{nT} \left| \sum_{i=0}^{\infty} \lambda^{(D-2)i} \sin(\lambda^i t) \right| dt} \tag{17}$$

Ra represents the simulated gear surface roughness, *T* is the meshing period of the gear system, and n signifies the number of cycles for system response simulation. In equation (17), the heights over the entire calculation period are integrated, resulting in the average height of all micro protrusions within the interval. Hence, the equation for simulating the tooth surface morphology can be expressed as:

$$z_1(t) = \frac{nTRa}{\int_0^{nT} \left| \sum_{i=0}^{\infty} \lambda^{(D-2)i} \sin(\lambda^i t) \right| dt} \sum_{i=0}^{\infty} \lambda^{(D-2)i} \sin(\lambda^i t) \tag{18}$$

According to the proposed modified equation, a simulation of a localized portion of the tooth surface was conducted. The simulation results of rough surface profile are shown in figure 2.

Based on figure 2, it can be observed that at the same fractal dimension, as the roughness increases, the peak height of the tooth surface micro-convex body increases, while the number of peaks and the frequency of fluctuations per unit area do not change significantly. On the other hand, under fixed roughness conditions, with the increase of fractal dimension, although the peak height of the micro-convex body on the tooth surface remains almost unchanged, the number of micro-convex body peaks per unit area significantly increases, showing more details on the tooth surface.

Therefore, the dynamic clearance of the gear pair is derived as follows:

$$z(t) = 2b_0 - \sum_{i=1}^{2} \left(\frac{nTRa_i}{\int_0^{nT} \left| \sum_{j=0}^{\infty} \lambda^{(D-2)j} \sin(\lambda^j t) \right| dt} \sum_{j=0}^{\infty} \lambda^{(D_i-2)j} \sin(\lambda^j t) \right) \tag{19}$$

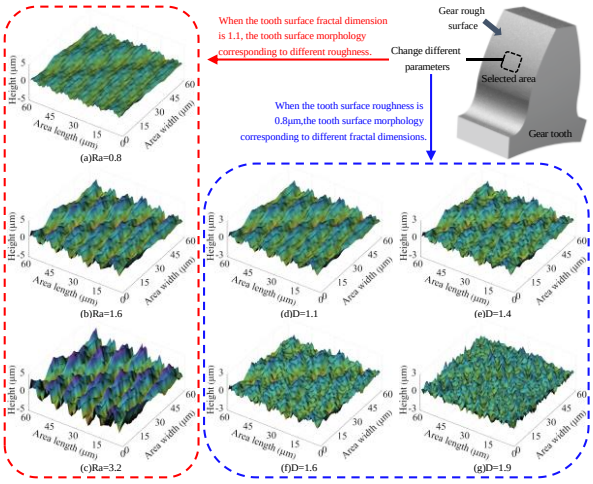

Figure 2. The two-dimensional simulation results of rough surface profile.

2.4.2 Multi-clearance coupling

The dynamic backlash caused by bearing clearance may lead to complex changes in the meshing forces. As shown in figure 3.

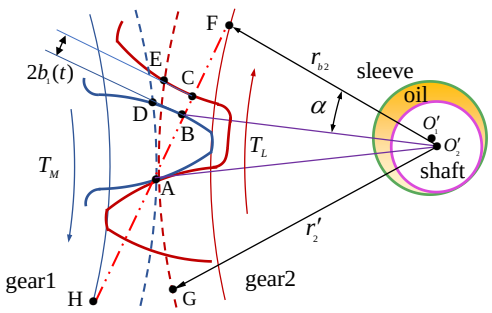

Figure 3. Geometrical relationship between gear backlash and center distance.

The initial center distance of the gear is expressed as follows:

$$a_s = (M_1 Z_1 + M_2 Z_2)/2 \tag{20}$$

where $M_i (i = 1,2)$ is the gear modulus, $Z_i (i = 1,2)$ is the number of gear teeth.

In the gear system, the gear backlash and bearing clearance will be coupled with each other, and the overall movement of the gear will cause the change of the center distance due to the bearing clearance, which affects the meshing line and the actual working pressure angle in turn. Then the actual center distance of the gear is expressed by:

$$a = \sqrt{(a_s + \Delta x_1 - \Delta x_2)^2 + (\Delta y_1 - \Delta y_2)^2} \tag{21}$$

The actual working pressure angle is as follows:

$$\alpha = \arccos((R_1 + R_2)/a) \tag{22}$$

Therefore, the dynamic backlash considering the fractal backlash is:

$$2b_1(t) = 2a\cos(\alpha)(\mathrm{inv}(\alpha) - \mathrm{inv}(\alpha_0)) + 2b_0 - \sum_{i=1}^{2}\left(\frac{nTRa_i}{\int_0^{nT} \left| \sum_{j=0}^{\infty} \lambda^{(D-2)j} \sin(\lambda^j t) \right| dt} \sum_{j=0}^{\infty} \lambda^{(D_i-2)j} \sin(\lambda^j t) \right) \tag{23}$$

It can be seen that considering the fractal dimension, roughness, bearing axis displacement and other nonlinear functions, the dynamic backlash is expressed. Compared with the traditional gear-bearing collision model, time-varying pressure angle and tooth-side fractal backlash and other nonlinear factors are taken into account for the subsequent study of gear models as a preparation.

2.5. Engagement model considering time-varying pressure and position angles

The gear dynamics parameters include time-varying meshing stiffness, meshing damping, dynamic backlash, etc. The gear meshing is described by a nonlinear stiffness $k_1(t)$ and viscous damping $c_1(t)$. The meshing stiffness of the tooth surface is described by using the method proposed in Ref. [19]. The meshing stiffness is expressed as:

$$k_1(t) = k_m(1 + k_c(t)) \tag{24}$$

where k_m is the averaged tooth stiffness, $k_c(t)$ is the variant part of the stiffness, in general it can be expanded in Fourier series.

The static transmission error $e_1(t)$ is a displacement excitation related to the manufacturing and installation accuracy of gears. It can usually be expressed by:

$$e_1(t) = e_m + \sum_{h=1}^{\infty} \left[e_{2h} \cos(h\omega_m t) + e_{2h+1} \sin(h\omega_m t) \right] \tag{25}$$

where e_m is the mean value of the meshing error, ω_m is the engagement frequency of the gear。

The meshing damping of the gears is given by [19]:

$$c_1 = 2\xi_2\sqrt{\frac{k_m J_1 J_2}{r_{b1}^2 J_2 + r_{b2}^2 J_1}} \tag{26}$$

where k_m is the average value of the time-varying meshing stiffness, ξ_2 is the gear meshing damping ratio, usually taken as 0.03~0.17 and the average value of 0.1 is taken in this paper.

Position angle β can be expressed by:

$$\beta = \tan^{-1}\frac{\Delta y_2 - \Delta y_1}{\Delta x_2 - \Delta x_1 + a_1} \tag{27}$$

q denotes the dynamic transfer error (DTE):

$$q = R_1\theta_1 - R_2\theta_2 + (\Delta x_1 - \Delta x_2)\sin(\alpha - \beta) + (\Delta y_1 - \Delta y_2)\cos(\alpha - \beta) - e(t) \tag{28}$$

The backlash nonlinear function of DTE is as follows:

$$g(q) = \begin{cases} q(t) - b_1(t) & q(t) > b_1(t) \\ 0 & -b_1(t) < q(t) < b_1(t) \\ q(t) + b_1(t) & q(t) < -b_1(t) \end{cases} \tag{29}$$

During gear meshing, the meshing force $F_p(t)$ consists of the elastic meshing force due to the time-varying meshing stiffness and the viscous meshing force due to the meshing damping. Then the meshing force is expressed as:

$$F_p(t) = k_1(t)g(q) + c_1\dot{q} \tag{30}$$

During the meshing process, the pressure angle and the position angle of the time change continuously. Therefore, the direction in which the meshing force and the friction force act on the gears are constantly changing. The force balance equation of the two gears in the *x* and *y* directions can be expressed as follows:

$$\begin{cases} m_1\Delta\ddot{x}_1 = -F_p(t)\sin(\gamma) + \bar{F}_{x1} + \tilde{F}_{x1} \\ m_1\Delta\ddot{x}_2 = F_p(t)\sin(\gamma) + \bar{F}_{x2} + \tilde{F}_{x2} \\ m_1\Delta\ddot{y}_1 = -F_p(t)\cos(\gamma) + \bar{F}_{y1} + \tilde{F}_{y1} \\ m_2\Delta\ddot{y}_2 = F_p(t)\cos(\gamma) + \bar{F}_{y2} + \tilde{F}_{y2} \end{cases} \tag{31}$$

where γ is the angle between the gear engagement line and the Y direction. γ can be expressed by $\gamma = \alpha - \beta$. The equilibrium equation of the two gears in the torsion direction can be expressed as follows:

$$\begin{cases} J_1\ddot{\theta}_1 = T_M - F_p(t)r_{b1} \\ J_2\ddot{\theta}_2 = T_L + F_p(t)r_{b2} \end{cases} \tag{32}$$

2.6. Principle and workflow of the proposed closed-loop algorithm

In contrast to the conventional approach of assuming a constant backlash, this study presents a computational model that incorporates dynamic fractal backlash. Based on the simulated time obtained previously, a modified equation for simulating the gear surface morphology is derived, taking into account the actual central displacement of the gear to calculate the actual backlash. Moreover, the proposed model introduces a damping coefficient that is dependent on the initial collision velocity, distinguishing it from existing bearing collision models. To account for this, it is necessary to update or inherit the damping coefficient at the beginning and end of each collision, and subsequently incorporate them

back into the dynamic equations. The dynamic equations of the system are then solved iteratively using a closed-loop algorithm. The overall procedure is illustrated in the flowchart depicted in figure 4.

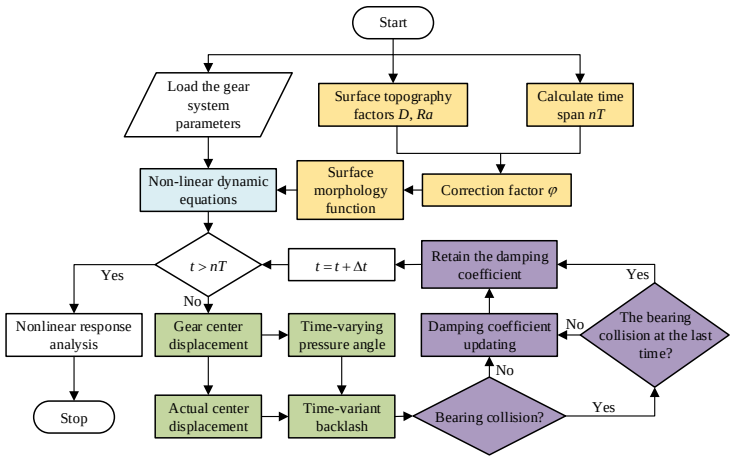

Figure 4. Flowchart of the proposed closed-loop algorithm.

3. COMPARISON AND DISCUSSION

The system model is solved using the aforementioned closed-loop algorithm. In order to avoid the influence of transient response on the solution results, the time range of the calculation examples is set to the first 4000 cycles, and the first 3000 cycles are ignored. In this section, a pair of parallel-axis involute spur gears is taken as an example and applied to the newly established improved model and other models for comparison. The specific parameters of the gear system are shown in table 1.

Table 1. Main parameters of the gear pair.

Name	Notation	Unit	Value
Tooth shape			Standard involute
Module	m	mm	3
Pressure angle	α_0	deg	20
Number of teeth	Z_1 / Z_2		40
Moment of inertia	m_1 / m_2	kg	1
Rotation inertia	J_1 / J_2	kg·m^2	2.23e-3
Profile shift coefficient	χ		0
Young's modulus	E	GPa	210
Poisson's ratio	v		0.3
Mean meshing stiffness	k_m	N/m	3.0e8
Meshing damping ratio	ξ_2		0.1
Dynamic viscosity	μ	Pa·s	2.28e-2

3.1. Affection of rotational speed

Rotational speed is one of the most important parameters that influence the gear dynamics. The global characteristics are studied by bifurcation diagram, the proportion of meshing states, the three-dimension frequency spectrum map and largest dynamic meshing force (LDMF), in which it is assumed that the surface roughness Ra is 0.8, and the fractal dimensions D1 and D2 are equal to 1.1. Three models are compared, including:

(1) The traditional model, where the bearing collision model of the gear system is based on the Kelvin model;

(2) The compared model, where the gear system adopts a new bearing collision model but without considering the nonlinear oil film force;

(3) The improved model, where the gear system adopts a new bearing collision model while also considering the nonlinear oil film force.

In order to compare the meshing forces on the teeth of these three models, *LDMF* of the tooth surface is defined as follow:

$$LDMF = \frac{\max[F_p(t)]}{F_s} \tag{33}$$

where F_s is the static meshing force, defined as the ratio of the average input torque to the gear base radius.

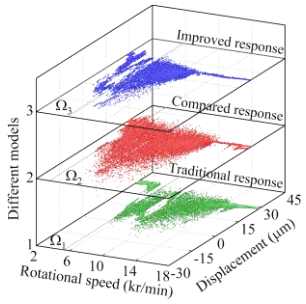

(a)Bifurcation diagram with the rotational speed

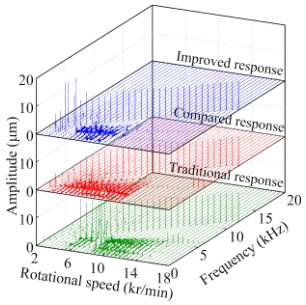

(b) Three-dimensional frequency spectrum map with the rotational speed

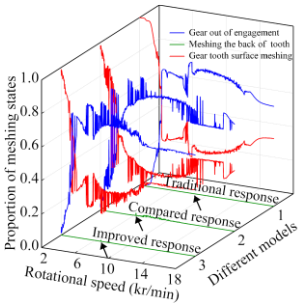

(c)Proportion of meshing states with the rotational speed

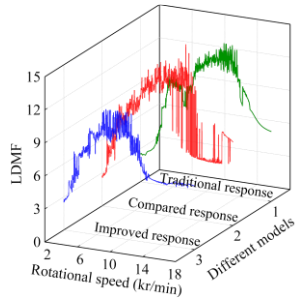

(d)Comparison of LDMFs under different rotational speed

Figure 5. Dynamic feature with varying rotational speed.

Through the analysis of bifurcation diagram and three-dimensional FFT spectrum, we can observe that as the rotational speed increases, the system response of the traditional model becomes chaotic at a speed of 5340r/min. The system response of the compared model and the improved model first enter chaotic state at rotational speeds of 3575r/min and 5725r/min respectively. Further observation of the bifurcation diagram shows that compared to the traditional model, the chaotic area size and response amplitude in the compared model increase. This indicates that the system response will enter chaotic state earlier with the application of the new collision bearing model as the rotational speed increases. Moreover, after considering the oil film force, the chaotic area of the improved model is smaller than that of the compared model, indicating that the stability of the system is improved. This is consistent with the actual situation and indirectly verifies the correctness of the model.

Compared to the traditional model, the dynamic transmission error (DTE) fluctuation amplitude of the improved and comparative models increases. As shown in figure 5(c), as the speed of the active wheel increases, the traditional model achieves 100% meshing ratio in the range of 2000 rpm to 2520 rpm. However, at a speed of 2000 rpm, the meshing ratio of the comparative and improved models is 97.9406% and 98.7719%, respectively. At 2520 rpm, the meshing ratio of the comparative and improved models is 87.8189% and 86.3783%, respectively. It is worth noting that there is no 100%

meshing ratio in the comparative and improved models within the speed range of 2000 rpm to 2520 rpm. Compared to the traditional model, the meshing ratio of the back teeth of the improved and comparative models appears earlier. In the traditional model, the back teeth meshing ratio first appears at 8740 rpm, accounting for 0.0266% of the entire meshing process. In the comparative model, the back teeth meshing ratio first appears at 5350 rpm, accounting for 0.0015% of the entire meshing process. In the improved model, the back teeth meshing ratio first appears at 6750 rpm, accounting for 0.7406% of the entire meshing process. It is obvious from figure 5(c) that the comparative model exhibits obvious back teeth meshing in the speed range of 6000 rpm to 12000 rpm. The maximum back teeth meshing ratio of the comparative model appears at 6250 rpm, accounting for 1.6718% of the total meshing time. The maximum back teeth meshing ratio of the improved model appears at 6750 rpm, accounting for 0.7406% of the total meshing time. The traditional model almost does not exhibit back teeth meshing in the range of 6000 rpm to 18000 rpm. The traditional model only exhibits back teeth meshing at speeds of 9940 rpm and 11640 rpm, accounting for 0.0406% and 0.0297%, respectively. It can be seen that with the increase of speed, the fluctuation amplitude of the meshing and separation ratios of the improved and comparative models is much greater than that of the traditional model.

According to figure 5(d), it can be observed that the adoption of the new bearing collision model resulted in an increase in LDMF (local dynamic load factor) to some extent. However, once the oil film force is taken into account, the LDMF in the entire speed range decreases to varying degrees. This indicates that the effect of the oil film force at the bearing leads to a decrease in the dynamic tooth meshing force of the gear system.

3.2. Gear dynamics influenced by oil film force

To compare the dynamic response of the three models, τ is defined as a dimensionless time. It can be expressed by:

$$\tau = t / T \tag{34}$$

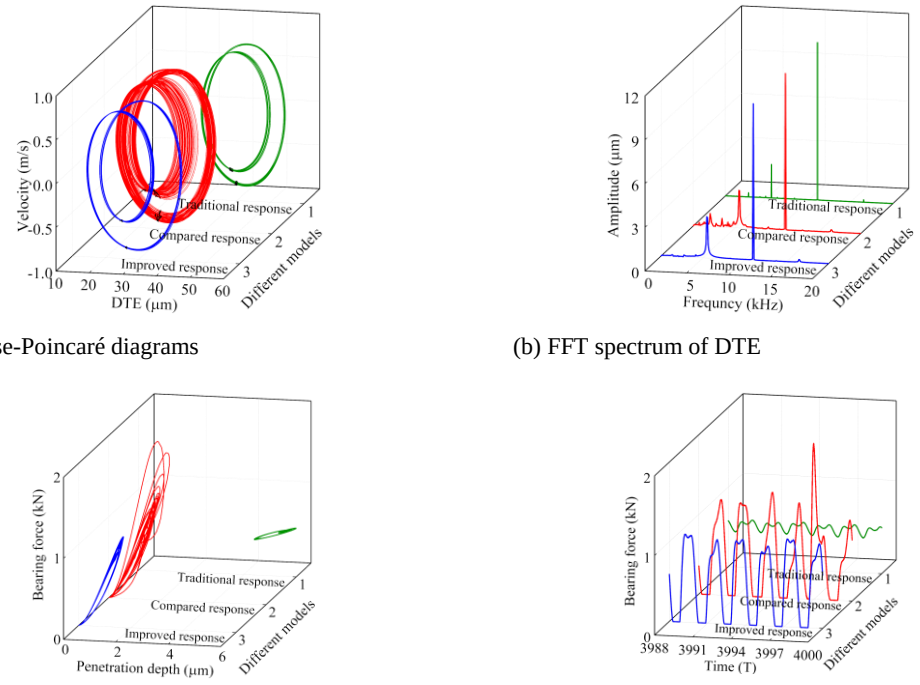

(a) Phase-Poincaré diagrams

(b) FFT spectrum of DTE

(c) The response of bearing force-displacement

(d) Diagram of bearing forces in the time domain

Figure 6. Dynamic feature with fractal backlash around n = 16.5kr/min.

Figure 6 illustrates the dynamic responses of the three models at a speed of 16.5kr/min. It can be observed that when considering only the new bearing collision model, the system response transitions from periodic to chaotic motion. However, with the further addition of oil film forces, the system response returns to periodic behavior. The traditional model exhibits a penetration depth range of 4.3875μm to 6.0145μm, while the comparative model's penetration depth range is from 0μm to 2.3108μm. With the inclusion of oil film, the penetration depth at the bearing location is further

reduced, resulting in a penetration depth range of 0μm to 1.7165μm for the improved model. The average bearing forces for the three models are 519.1513 N, 374.1020 N, and 353.5846 N, respectively, while the maximum bearing forces increase from 604.0786 N to 1956.5671 N and 1121.2492 N for the comparative and improved models. Although the traditional model exhibits larger average bearing outer ring penetration depth and bearing forces compared to the improved and comparative models, its fluctuation range of bearing forces is smaller. The bearing force curves of the improved and comparative models reveal frequent collisions and separations between the bearing and the outer ring, which is not observed in the traditional model. In the frequency domain, the comparative model shows more subharmonic components in its response, but these components decrease significantly with the addition of oil film forces. Further comparison between the improved and comparative models shows a decrease in maximum penetration depth of the bearing by 0.5943μm and a decrease in maximum bearing force by 835.3179 N when oil film forces are added. This indicates that the inclusion of oil film forces leads to a decrease in the maximum values of bearing force and penetration depth. Compared to the traditional bearing collision model, the newly proposed bearing collision model exhibits more nonlinear characteristics. Therefore, it is recommended to consider oil film effects and adopt the Hertz contact model, rather than the Kelvin model, in the bearing collision model when modeling gear dynamics.

3.3. Gear dynamics influenced by restitution coefficient

First set the parameter size as follows: $b_0 = 50\mu\text{m}$, $T_M = 30\text{N}\cdot\text{m}$, $\xi_2 = 0.1$, $\omega = 15000\text{rpm}$, $R_a = 0.8$, $D = 1.1$.

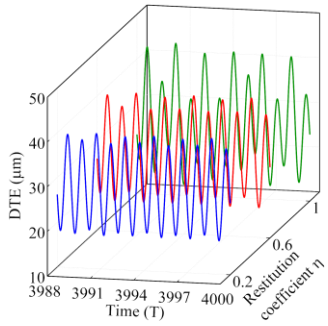

(a) Time-domain plot

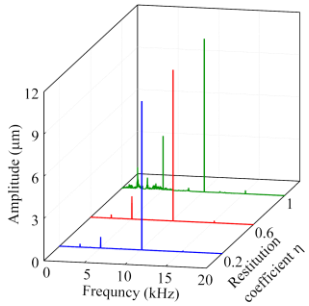

(b) FFT spectrum of DTE

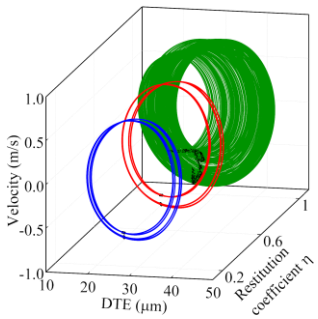

(c) Phase diagram and time-frequency Poincaré map

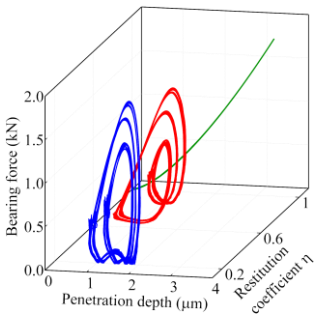

(d) The response of bearing force-displacement

Figure 7. Dynamic characteristic by different fractal parameter.

The results are presented in figure 7. As the restitution coefficient increases, the area enclosed by the hysteresis loop of the bearing force gradually decreases and ultimately becomes a curve when the restitution coefficient reaches 1. At the same time, the amplitude range of DTE increases with the increase of the restitution coefficient. For example, when the restitution coefficient is 0.2, the fluctuation range of DTE is 17.4948μm to 40.2586μm. When the restitution coefficient is 0.6, the fluctuation range of DTE changes to 16.6860μm to 41.0608μm, and when the restitution coefficient is 1, the fluctuation range of DTE changes to 12.4809μm to 43.8921μm. Figure 7(c) shows that as the restitution coefficient increases, the Poincaré points become more dispersed, and the system response trajectory becomes thicker. In the frequency domain, more subharmonic components of DTE appear, and the corresponding amplitudes also increase. This indicates that the stability of the system response decreases as the restitution coefficient increases. The trend of the bearing

force with the restitution coefficient is shown in figure 7. In order to compare the trend of the bearing force with the restitution coefficient, a dimensionless parameter λ_i is defined. λ_i can be expressed by:

$$\lambda_i = \frac{\varsigma_i}{\max(\varsigma_i)} \tag{35}$$

where the set of results for parameter ς_i, which requires non-dimensional processing, is presented.

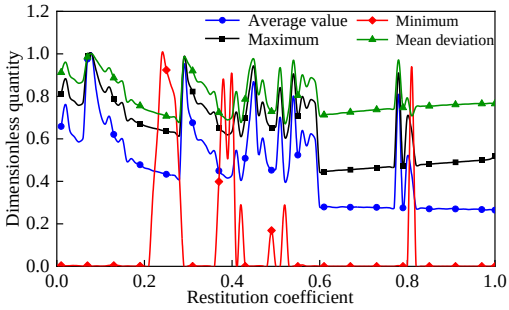

Figure 8. Dynamic characteristic by different fractal parameter.

From figure 8, it can be observed that when the restitution coefficient is 0.08, both the maximum and mean values of the bearing force reach their maximum values. In addition, in some intervals shown in the figure, the minimum bearing force is zero, indicating a separation phenomenon between the shaft and the outer ring of the bearing during the gear meshing process. This suggests that even if the elastic modulus and Poisson's ratio of the bearing material do not change, changing only the restitution coefficient can have a significant impact on the numerical values of bearing impact forces and the collision state between the shaft and the bushing during the gear meshing process. Therefore, it is crucial to choose an appropriate restitution coefficient when conducting collision simulations. The correct choice can ensure the accuracy and reliability of the simulation results.

3.4. Gear dynamics influenced by fractal dimension and surface roughness

In this section, we will explore the impact of tooth surface morphology as an important excitation inside the gear system on the system's nonlinear response. Fractal characteristics of the tooth surface morphology have time-varying and random properties, which can effectively describe the variation of tooth clearance in the gear transmission process. Our aim is to investigate the influence of tooth surface roughness and fractal dimension on system response. The set parameters are as follows: $b_0 = 50\mu\text{m}$, $T_M = 30\text{N}\cdot\text{m}$, $\xi_2 = 0.1$, $\omega = 15500\text{rpm}$.

The system response varies with the change in fractal dimension and roughness of the tooth surface, as shown in figure 9. The upper part of figure 9 shows the system response variation with increasing roughness, and the lower part shows the system response variation with changing fractal dimension. When the roughness is 0.8, the fluctuation range of DTE is from 17.7342μm to 39.9415μm. When the roughness is 1.6, the fluctuation range of DTE is from 17.7285μm to 42.0288μm. When the roughness is 3.2, the fluctuation range of DTE is from 17.4548μm to 45.5643μm. As the roughness increases, the amplitude range of the system response also increases. In addition, as the roughness increases, more sub-harmonic components appear in the frequency domain of DTE. In figure 8(c), we can see that with the increase of roughness, the system response trajectory gradually separates and changes from thin to thick, and the Poincaré points gradually become dispersed from being aggregated. The variation of dynamic pressure angle also changes from periodic response to chaotic response. Therefore, the system response undergoes a transition from double periodic response to chaotic response.

From the lower part of figure 9, it can be seen that the variation of system response is not obvious with the change of fractal dimension. When the fractal dimension is 1.1, the fluctuation range of DTE is from 17.7342μm to 39.9415μm. When the fractal dimension is 1.5, the fluctuation range of DTE is from 17.3602μm to 39.9969μm. When the fractal dimension is 1.9, the fluctuation range of DTE is from 17.6256μm to 39.0442μm. With the increase of fractal dimension, the amplitude range of the system response slightly decreases, and the trajectory of the system response in the phase diagram gradually becomes thicker, and the stability of the system response decreases. However, the system response is still a periodic response.

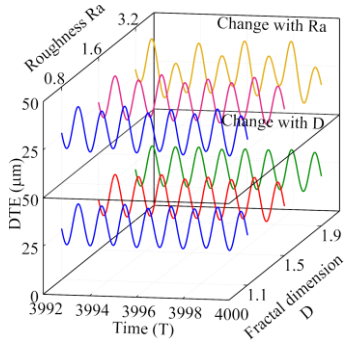

(a) Time-domain plot

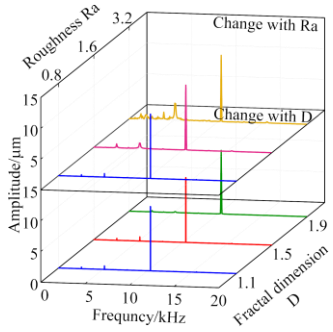

(b) FFT spectrum of DTE

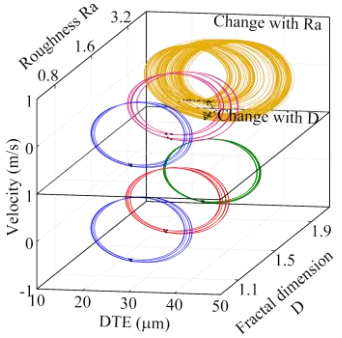

(c) Phase diagram and time-frequency Poincaré map

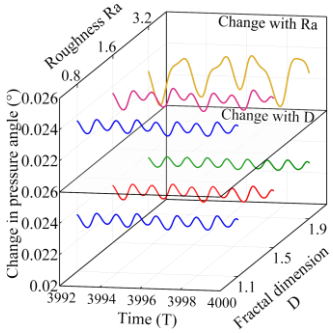

(d) The response of pressure angle

Figure 9. Dynamic characteristic by different surface roughness.

Based on the fractal theory of tooth surface morphology, we can see that increasing the fractal dimension slightly reduces the amplitude range of DTE. Increasing the tooth surface roughness will enlarge the amplitude range of DTE and make the system response more chaotic. Although the fractal dimension will decrease the transmission stability of the gear system to some extent, the influence of tooth surface roughness on transmission stability is more significant. Therefore, when considering improving the transmission stability of the gear, we should prioritize reducing tooth surface roughness.

4. CONCLUSION

Based on the proposed fractal tooth gap and bearing collision models, this study established a refined gear dynamic model. Considering the specific characteristics of factors such as viscous damping and time-varying pressure angle, a closed-loop algorithm is proposed to solve the system response. Through a comparative analysis of the improved model with traditional models and an examination of the effects of different parameters on the system response. The main conclusions are as follow:

(1) The adoption of the novel bearing collision model resulted in an earlier onset of chaotic behavior in the gear system compared to traditional models. Within the speed range of 6000rpm to 12000rpm, the chaotic region significantly expanded, accompanied by notable instances of gear back engagement. Moreover, an increased oil film force improved the stability of the system response, with some regions transitioning from chaotic to multi-periodic responses.

(2) The coefficient of restitution during the bearing collision process exerted a significant influence on the magnitude of bearing forces and the stability of the system response. As the coefficient of restitution increased, the energy dissipation during a single collision process decreased, leading to reduced stability of the system response and increased fluctuation of DTE. Therefore, selecting an appropriate coefficient of restitution is crucial in accurately describing energy dissipation and system response during collisions in gear system simulations.

(3) When describing tooth surface morphology using fractal theory, an increase in both tooth surface roughness and fractal dimension resulted in wider DTE phase orbits and more dispersed Poincaré points, thereby decreasing system stability.

However, tooth surface roughness had a more significant impact on system stability compared to the influence of fractal dimension.

REFERENCES

[1] Xiao H, Zhou X, Liu J and Shao Y 2017 Vibration transmission and energy dissipation through the gear-shaft-bearing-housing system subjected to impulse force on gear *Measurement* **102**: 64-79.

[2] Ryali L and Talbot D 2021 A dynamic load distribution model of planetary gear sets *Mechanism and Machine Theory* **158**: 104229.

[3] Chowdhury S and Yedavalli R K 2017 Dynamics of low speed geared shaft systems mounted on rigid bearings *Mechanism and Machine Theory* **112**: 123–144.

[4] Guan D, Jing L, Gong J and Shen H 2018 Normal contact analysis for spherical pump based on fractal theory *Tribology International* S0301679X18301890.

[5] Litak G and Friswell M I 2003 Vibration in gear systems *Chaos Solitons Fractals* **16**: 795–800.

[6] Humphrey E, Morris N J, Rahmani R and Rahnejat H 2020 Multiscale boundary frictional performance of diamond like carbon coatings *Tribology International* 149105539.

[7] Chen Q, Yunbo M, Shouwu H, et al. 2014 Research on gears' dynamic performance influenced by gear backlash based on fractal theory *Applied Surface Science* **313**: 325-332.

[8] Chen Q, Zhou J, Khushnood A, et al. 2019 Modelling and nonlinear dynamic behavior of a geared rotor-bearing system using tooth surface microscopic features based on fractal theory *AIP Advances*.

[9] Xiang L, Zhang Y, Gao N and Hu A 2018 Nonlinear dynamics of a multistage gear transmission system with multi-clearance *International Journal of Bifurcation and Chaos*.

[10] Yu X, Sun Y, Li H, et al. 2022 Nonlinear characteristics of gear pair considering fractal surface dynamic contact as internal excitation. *International Journal of Non-Linear Mechanics* **143**: 104027.

[11] Pan W, Ling L, Qu H, et al. 2022 Early wear fault dynamics analysis method of gear coupled rotor system based on dynamic fractal backlash *Journal of Computational and Nonlinear Dynamics* **17**(1): 011003.

[12] Chen Q, Wang Y, Tian W et al. 2019 An improved nonlinear dynamic model of gear pair with tooth surface microscopic features *Nonlinear Dynamics* **96**: 1615-1634.

[13] Han J, Li G and Tian X 2023 Nonlinear dynamics analysis of gear transmission system based on tooth surface microtopography *Journal of Vibration Engineering & Technologies*.

[14] Yu J, Wang H and Ren D 2022 Chaos analysis of single-stage spur gear system considering backlash fractal *Journal of Vibration Engineering & Technologies*: 1-11.

[15] Huang K, Cheng Z, Xiong Y and Han G 2020 Bifurcation and chaos analysis of a spur gear pair system with fractal gear backlash *Chaos Solitons & Fractals* **142**: 110387.

[16] Liu Z, Liu Z, Zhao J, et al. 2017 Study on interactions between tooth backlash and journal bearing clearance nonlinearity in spur gear pair system *Mechanism and Machine Theory* **107**: 229-245.

[17] Zhang R, Wang K, Shi Y and Sun X 2019 The influences of gradual wears and bearing clearance of gear transmission on dynamic responses *Energies* **12.**

[18] Kim W, Yoo H and Chung J 2010 Dynamic analysis for a pair of spur gears with translational motion due to bearing deformation *Journal of Sound & Vibration* **329**(21): 4409-4421.

[19] Guo D, Ning Q and Ge S 2022 Nonlinear characteristic analysis of gear rattle based on refined dynamic model *Nonlinear Dynamic* **110**: 3109–3133.

[20] Gilardi G and Sharf I 2002 Literature survey of contact dynamics modelling *Mechanism and Machine Theory* **37**(10): 1213-1239.

[21] Lankarani H M and Nikravesh P E 1994 Continuous contact force models for impact analysis in multibody systems *Nonlinear Dynamics* **5**: 193-207.

[22] Machado M, Moreira P, Flores P et al. 2012 Compliant contact force models in multibody dynamics: Evolution of the Hertz contact theory *Mechanism and Machine Theory* **53:** 99-121.

[23] Capone G, Russo M and Russo R 1987 Dynamic characteristics and stability of a journal bearing in a non-laminar lubrication regime *Tribology International* **20**(5): 255-260.